Acta Crystallographica Section B
Structural Science
ISSN 0108-7681

Synchrotron X-ray study of $Er_3Al_5O_{12}$ and $Yb_3Al_5O_{12}$ garnets

Barbara Etschmann,[a]* Victor Streltsov,[b] Nobuo Ishizawa[a] and E. N. Maslen[b]†

[a]Materials and Structures Laboratory, Tokyo Institute of Technology, 4259 Nagatsuta, Midori-ku, Yokohama 226-8503, Japan, and [b]Crystallography Centre, University of Western Australia, Nedlands 6907, Australia

† Deceased.

Correspondence e-mail: bee@r3401.rlem.titech.ac.jp

Received 18 July 2000
Accepted 7 December 2000

Structure factors for $Er_3Al_5O_{12}$ and $Yb_3Al_5O_{12}$ garnets were measured using focused synchrotron X-radiation, with λ = 0.7500 (2) and 0.7000 (2) Å, respectively. The difference electron density maps for $Er_3Al_5O_{12}$ and $Yb_3Al_5O_{12}$ were similar, as expected. This was attributed to the 4*f* electrons being shielded, which reduces their effectiveness in chemical bonding and the relative position of the rare-earth atoms in the periodic table. The symmetry of the difference electron density around the rare-earth atoms was found to reflect that of the cation geometry, emphasizing the importance of second nearest-neighbor interactions. This is consistent with the view that oxide-type structures may be regarded as a packed array of cations with anions in the interstices.

1. Introduction

Recent studies of oxide-type structures with metals in low-symmetry positions, *e.g.* perovskite-type structures, have revealed that a local difference electron density near the cations has a symmetry higher than the crystallographic symmetry (*e.g.* Maslen *et al.*, 1995). The higher local symmetry matches that of the next nearest cations, emphasizing the long-range effects that cations (or the less electronegative atoms) have on the structure of non-molecular crystals. This is consistent with O'Keeffe & Hyde's (1981) view that oxide-type structures may be considered as a packed array of cations with anions inserted into the interstices. Accurate difference electron density ($\Delta\rho$) studies of structures with metals in low-symmetry positions have now been extended to include rare-earth garnets, which have the rare-earth (RE) in the 2.22 position in $Ia\bar{3}d$.

Garnets are generally cubic with space group $Ia\bar{3}d$ and may be characterized by the formula $\{A_3\}[B_2](C_3)O_{12}$ (Geller, 1967), where the brackets reflect the oxygen coordination of the cation: {} indicates eightfold coordination of the rare-earth; [] sixfold coordination of Al(1) and () fourfold coordination of Al(2). The garnet structure may be visualized following the description given by Hyde & Andersson (1989). They used a b.c.c. (body-centred cubic) rod packing scheme, where a rod was defined to consist of alternating face-sharing octahedra and trigonal prisms. The rods are parallel to one of the four body-diagonals of the cubic cell. The octahedral cations Al(1) [in special position 16(*a*)] are located at the centers of O_6 octahedra and the trigonal prisms are empty. The Al(2) atoms lie in the tetrahedral interstices located between the polyhedral rods and the RE atoms are inside a distorted cube of O atoms.

Alternatively, garnets can be viewed as 'oxygen-stuffed alloys' (O'Keeffe & Hyde, 1981) when described in terms of

the cation subnet (Fig. 1). Ramos-Gallardo & Vegas (1997) extended the O'Keeffe and Hyde view by noting that a close relationship exists between the RE subarray in garnets and the parent metallic phase. The RE–RE distances are similar to those found in elemental RE (Ramos-Gallardo & Vegas, 1997) and RE—Al distances are close to those in Al_3RE and RE_3Al alloys. The Al subarray cannot be related to metallic aluminium, as the Al—Al distances in the garnets are considerably larger than those found in elemental Al (2.86) Å (Ramos-Gallardo & Vegas, 1997). This, combined with the difficulty in obtaining RE—RE distances less than those in the elemental form, forces the Al subnet to expand and accommodate the RE—Al and RE—RE distances. Thus, there is no evidence of the metallic aluminium structure in the garnet structure. Therefore, the cation arrays can be considered as a distortion of the elemental parent structure or Al—RE alloys, which resulted from the inclusion of other atoms or groups. These metal–metal interactions should affect the electron density distribution.

2. Experimental

Single crystals of $Er_3Al_5O_{12}$ and $Yb_3Al_5O_{12}$ were prepared using a flux technique similar to that described by Remeika & Kometani (1968). Rare earth oxide and PbO powders were mixed in a 1:6 weight ratio, with 0.0015 *M* of Al_2O_3 (Garton & Wanklyn, 1967). This mixture was held in a furnace at ~1500 K for 1 h, cooled to 1123 K at 40 K h^{-1} and then rapidly cooled to room temperature. The final mixture was simmered with dilute HNO_3 to dissolve the PbO flux. Garnet crystals were multi-faceted and ranged in size, from ~30 to 100 μm. The $Er_3Al_5O_{12}$ had a red tinge, while the $Yb_3Al_5O_{12}$ crystals were colorless.

The sample of $Er_3Al_5O_{12}$ selected for X-ray analysis was roughly a rectangular plate with the corners removed and had approximately 17 faces. The major faces were $\{\bar{2}\bar{1}1\}$, {011}, $\{1\bar{1}1\}$, {110} and $\{10\bar{1}\}$. The distances from the origin to the bounding faces were, respectively, 0.021 (1), 0.010 (1), 0.007 (1), 0.020 (1) and 0.021 (1) mm. This crystal did not conform to any of the typical garnet shapes (Dana, 1954). The $Yb_3Al_5O_{12}$ crystal appeared to be a fairly regular dodecahedron with the edges cut off. The faces were {101}, {011}, {110}, {101}, {110} and {011}, with an origin-to-bounding face distance of 0.025 (1) mm. Crystal dimensions were determined with the electroscan scanning electron microscope (ESEM).

Diffraction data sets for both garnets were collected on the beamline BL 14 A four-circle diffractometer at the Photon Factory in Tsukuba, Japan (Satow & Iitaka, 1989). BL 14A is equipped with a vertical wiggler and the subsequent vertically polarized radiation is passed through a double Si(111) crystal monochromator, which is focused using a curved mirror. The polarization ratio, which is the fraction of the total incident intensity that has a vertical electric vector, is 0.95. A 0.4 mm diameter slit situated in front of the ion-counter monitor ensures the beam is intense and adequately homogeneous. The stored electron beam was monitored with an ion chamber. The intensity of the synchrotron beam can slightly fluctuate due to particle beam instabilities and the thermal instability of beamline optics, however, the effects of this can be minimized by positioning the crystal slightly off the beam focus.

Lattice constants for $Er_3Al_5O_{12}$ and $Yb_3Al_5O_{12}$ were determined from 14 reflections with 2θ values in the ranges 77.420–81.060 and 55.960–75.075°, respectively. The $\omega/2\theta$ scan was used to measure reflection intensities over a full sphere of reciprocal space up to $(\sin\theta/\lambda)_{max}$ = 1.125 $Å^{-1}$ for $Er_3Al_5O_{12}$ and 1.094 $Å^{-1}$ for $Yb_3Al_5O_{12}$.

The $Yb_3Al_5O_{12}$ data set was collected with a NaI scintillation detector. The deadtime for the NaI counter has been measured to be 1.2 ms. To minimize deadtime losses, strongly diffracting intensities with count rates higher than 60 000 c.p.s. were reduced with a Pt foil, which had an attenuation factor of 47.45 at 0.7000 (2) Å. These deadtime counting losses were further corrected using the polynomial expansion as in Hester *et al.* (1993*a*,*b*).

The $Er_3Al_5O_{12}$ data set was collected using a fast Avalanche Photodiode Detector (APD) recently installed at BL 14 A (Kishimoto, 1995; Streltsov *et al.*, 1998). With a relatively high intrinsic efficiency of 55% at 0.7500 (2) Å, the APD has a dynamic range up to 10^8 c.p.s.

Reasons for using the wavelengths of 0.7 and 0.75 Å were the greater stability of the experimental equipment at the setting in this range of wavelengths and the higher intensity of radiation to improve the measurements of a considerable amount of weak reflections. The already fixed energies to 17 711 and 16 531 eV were used owing to limited time at the beamline during two experimental sessions. The calibration of wavelengths using a single crystal of silicon and the estimation of the energy resolution less than 2 eV gave the wavelengths of 0.7000 (2) and 0.7500 (2) Å.

Six standards were measured every 100 reflections, to monitor the stability of the incident beam. Variation in the standards due to beam instabilities allow measured intensities to be modified accordingly and indicate how variances in the

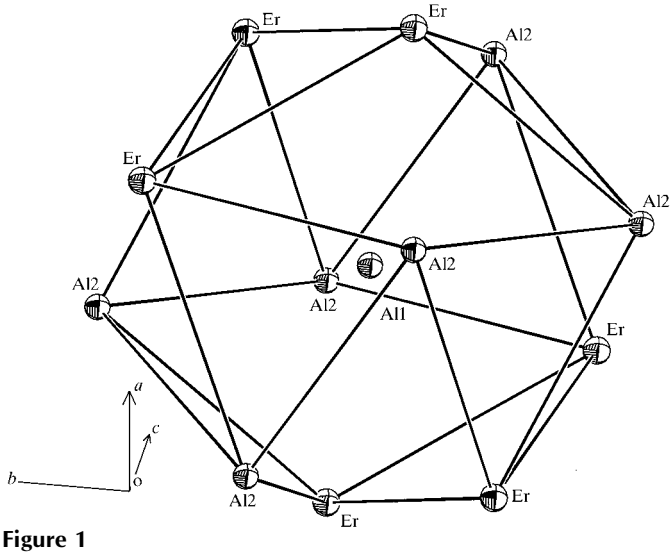

Figure 1
The 12-coordinated Al(1)-icosahedron: cation subnet in garnet structure. The *c* axis is directed towards the reader.

Table 1
Experimental details.

	$Er_3Al_5O_{12}$	$Yb_3Al_5O_{12}$
Crystal data		
Chemical formula	$Al_5Er_3O_{12}$	$Al_5O_{12}Yb_3$
Chemical formula weight	828.68	846.02
Cell setting, space group	Cubic, $Ia\bar{3}d$	Cubic, $Ia\bar{3}d$
a, b, c (Å)	11.9928 (2), 11.9928 (2), 11.9928 (2)	11.9386 (4), 11.9386 (4), 11.9386 (4)
V (Å^3)	1724.89 (9)	1701.6 (3)
Z	8	8
D_x (Mg m^{-3})	6.382	6.605
Radiation type	Synchrotron	Synchrotron
Wavelength (Å)	0.7500 (2)	0.7000 (2)
No. of reflections for cell parameters	14	14
θ range (°)	77.420–81.060	55.960–75.075
μ (mm^{-1})	32.72	30.95
Temperature (K)	293	293
Crystal form, color	Rectangular plate, light red	Dodecahedron, colorless
Crystal size (mm)	0.021 × 0.020 × 0.013	0.050 × 0.050 × 0.050
Data collection		
Diffractometer	BL14A	BL14A
Data collection method	$\omega/2\theta$ scans	$\omega/2\theta$ scans
Absorption correction	Analytical (Alcock, 1974)	Analytical (Alcock, 1974)
T_{min}	0.41	0.29
T_{max}	0.66	0.35
No. of measured, independent and observed parameters	38 377, 866, 866	34 089, 788, 788
Criterion for observed reflections	$F > 3\sigma(F)$	$F > 3\sigma(F)$
R_{int}	0.09	0.089
θ_{max} (°)	57.41	49.96
Range of h, k, l	$-26 \rightarrow h \rightarrow 26$ $-26 \rightarrow k \rightarrow 26$ $-26 \rightarrow l \rightarrow 26$	$-26 \rightarrow h \rightarrow 26$ $-26 \rightarrow k \rightarrow 26$ $-26 \rightarrow l \rightarrow 26$
No. and frequency of standard reflections	6 every 94 reflections	6 every 94 reflections
Intensity decay (%)	1	1
Refinement		
Refinement on	F	F
R, wR, S	0.022, 0.028, 3.097	0.022, 0.031, 3.453
No. of reflections and parameters used in refinement	866, 16	765, 16
Weighting scheme	σ	σ
$(\Delta/\sigma)_{max}$	0.001	0.0001
$\Delta\rho_{max}$, $\Delta\rho_{min}$ (e Å^{-3})	2.1, −4.8	2.2, −3.6
Extinction method	Zachariasen (1967)	Zachariasen (1967)
Extinction coefficient	0.35 (7) × 10^4	0.49 (5) × 10^4

Computer programs used: *XtalDIFDATADDREFSORTRFABSORB*, *XtalCRYLSQ*, *XtalBONDLACIFIO* (Hall *et al.*, 1995).

structure factors due to counting statistics should be adjusted (Rees, 1977). Other experimental parameters are listed in Table 1.

Lorentz and polarization corrections were applied, and absorption correction factors (Alcock, 1974) were evaluated analytically. The reference state for all structure-factor calculations was the independent atom model (IAM) evaluated using spherical atomic scattering factors with dispersion corrections $\Delta f'$ and $\Delta f''$ of −0.2877 and 5.437 for Er at 0.7500 Å, and −0.246 and 5.453 for Yb at 0.7000 Å calculated by Creagh (1995/1996). The other dispersion corrections $\Delta f'$, $\Delta f''$ of 0.0434, 0.058 and 0.0635, 0.050 for Al at 0.7500 and 0.7000 Å, respectively, and of 0.0118, 0.007 and 0.0108, 0.006 for O at 0.7500 and 0.7000 Å, respectively, were interpolated from *International Tables for X-ray Crystallography* (1974, Vol. IV).

All structures were refined using the *Xtal*3.4 (Hall *et al.*, 1995) system of crystallographic programs. Applying an isotropic Zachariasen (1967) extinction correction resulted in y_{min} = 0.76 and 0.71 for the Er and Yb garnets, respectively. To further evaluate the extinction correction, atomic charges were calculated by a Hirshfeld partitioning (Hirshfeld, 1977) of the difference density with respect to the free atom density. The charges were Er = −0.2 (2), Al(1) = 0.4 (2), Al(2) = 0.9 (2), O = −0.3 (2) and Yb = 1.0 (1), Al(1) = −0.1 (1), Al(2) = 0.4 (1), O = −0.3 (1). An isotropic Type I Becker–Coppens extinction correction gave y_{min} = 0.73 and 0.71 for Er and Yb garnets. The charges were Er = −0.2 (2), Al(1) = 0.5 (2), Al(2) = 0.8 (2), O = −0.2 (2) and Yb = 0.7 (1), Al(1) = 0.1 (1), Al(2) = 0.4 (1) and O = −0.3 (1). An isotropic Type II Becker–Coppens extinction correction gave y_{min} = 0.77 and 0.73 for Er and Yb garnets. The charges were Er = 2.6 (2), Al(1) = 0.02 (25), Al(2) = 0.5 (2) and O = −0.8 (2) and Yb = 2.1 (1), Al(1) = 0.3 (1), Al(2) = 1.2 (1) and O = −0.9 (1).

The magnitude of the extinction correction for all three methods is similar, however, both the Zachariasen and Becker–Coppens Type I (BCI) extinction refinement result in negative charges for Er, while the Becker–Coppens Type II (BCII) extinction correction gives positive charges for all cations and negative charges for the anion. Initially, it appears that the BCII extinction correction is the most appropriate. However, as a few low-angle reflections with high weights dominated the least-squares residual, further investigation was necessary. It has been noted previously that the extinction parameter is strongly correlated with the scale factor and the dominance of these residuals could be reduced by separate adjustment of both parameters (*e.g.* du Boulay *et al.*, 1995). A scale was determined first by refining the structure (without applying an extinction correction) with $\sin\theta/\lambda > 0.25$ Å^{-1}. With the scale fixed at the first stage value, the isotropic Zachariasen (1967) BCI and BCII extinction parameter was refined. The Zachariasen (1967) extinction correction resulted in y_{min} = 0.87 and 0.79 for the Er and Yb garnets, respectively. The charges were Er = 0.5 (3), Al(1) = 0.1 (3), Al(2) = 1.4 (3), O = −0.5 (2) and Yb = 1.4 (1), Al(1) = −0.6 (1), Al(2) = 1.0 (1), O = −0.5 (1). A BCI extinction correction gave y_{min} = 0.85 and 0.76 for Er and Yb garnets. The charges were Er = 0.5 (3), Al(1) = 0.1 (3), Al(2) =

1.4 (3), O = −0.5 (2) and Yb = 1.1 (1), Al(1) = −0.4 (1), Al(2) = 0.7 (1) and O = −0.4 (1). A BCII extinction correction gave y_{min} = 0.93 and 0.88 for Er and Yb garnets. The charges were Er = 1.9 (3), Al(1) = −0.3 (3), Al(2) = 1.4 (3) and O = −0.8 (2) and Yb = 2.3 (1), Al(1) = −0.5 (1), Al(2) = 2.0 (1) and O = −1.0 (1). Thus, applying the Zachariasen or the BCI extinction correction results in negative charges for anions and positive charges for cations, with the exception of Al(1) in the Yb-garnet. However, in the Er-garnet the Al(1) charge is positive but within one s.u. The BCII extinction correction gives negative charges for Al(1) in both garnets. It should be noted that charges determined by the spatial distribution of electrons are not the same as formal charges which relate to changes in the spin state of the electron.

The simpler Zachariasen (1967) extinction correction was used for the refinement. The isotropic Zachariasen (1967) extinction parameter and independent structural parameters, including all anisotropic vibration tensor elements, determined by full-matrix least squares refinement of $|F|$ with all measured structure factors weighted by $1/\sigma^2(F_o)$, are listed in Table 1.[1]

3. Structural and atomic displacement parameters

The unit-cell parameters for the two garnets agree well with those determined by Rubenstein & Barns (1964, 1965). They reported that a ($Er_3Al_5O_{12}$) = 11.981 (3) Å and a ($Yb_3Al_5O_{12}$) = 11.929 (3) Å, compared with the unit-cell lengths of 11.9928 (2) and 11.9386 (4) Å, respectively (Table 1). The Er garnet has a slightly larger unit cell than the Yb garnet, which is consistent with the Rubenstein & Barns (1964, 1965) observation that the unit-cell parameters of the rare-earth aluminium garnets decrease across the row. This conforms to the lanthanide contraction, which occurs due to the imperfect shielding of the 4*f* electrons.

The following trends in the atomic displacement parameters, which have been deposited, are observed for both garnets: for the rare earth atoms and Al(2): U^{22} (= U^{33}) > U^{11} and for O: $U^{22} > U^{11} > U^{33}$. The atomic displacement parameters can be related to the structure of the garnet. This can be seen most simply from Fig. 2, which indicates structural cavities in the [001] direction. (Atoms within +/− 4 Å of the plane are projected onto the plane.) Large vibrations of the RE and Al(2) atoms are observed in that direction. The Al(2) and RE atoms are packed relatively tightly along the [100] direction, subsequently constraining the vibration.

From Fig. 1 it can be seen that the metallic subnet can be broken into a number of subunits. The Al(1) atoms, which are arranged in a b.c.c. configuration throughout the garnet structure, are situated in the centre of an icosohedron formed by RE and Al(2) atoms. The main region of interest is the RE_3 plane, containing the three rare-earth atoms. The RE—RE distances in elemental Er and Yb, calculated from atomic positions and unit-cell parameters taken from Wyckoff (1963), are 3.8524 and 3.8793 Å, respectively. These values are approximately 0.2 Å longer than the experimental Er—Er and Yb—Yb bond distances listed in Table 2. This substantiates Ramos-Gallardo & Vegas' (1997) observation that the RE—RE distances in garnets are similar to those in the elemental RE. However, the shortest Al—Al distance, that between Al(1) and Al(2), is 3.3521 (3) and 3.3370 (2) Å in the Er and Yb garnets, respectively, compared with 2.86 Å in elemental Al. Thus, there is no evidence of the elemental Al structure in the garnet, as noted by Ramos-Gallardo and Vegas.

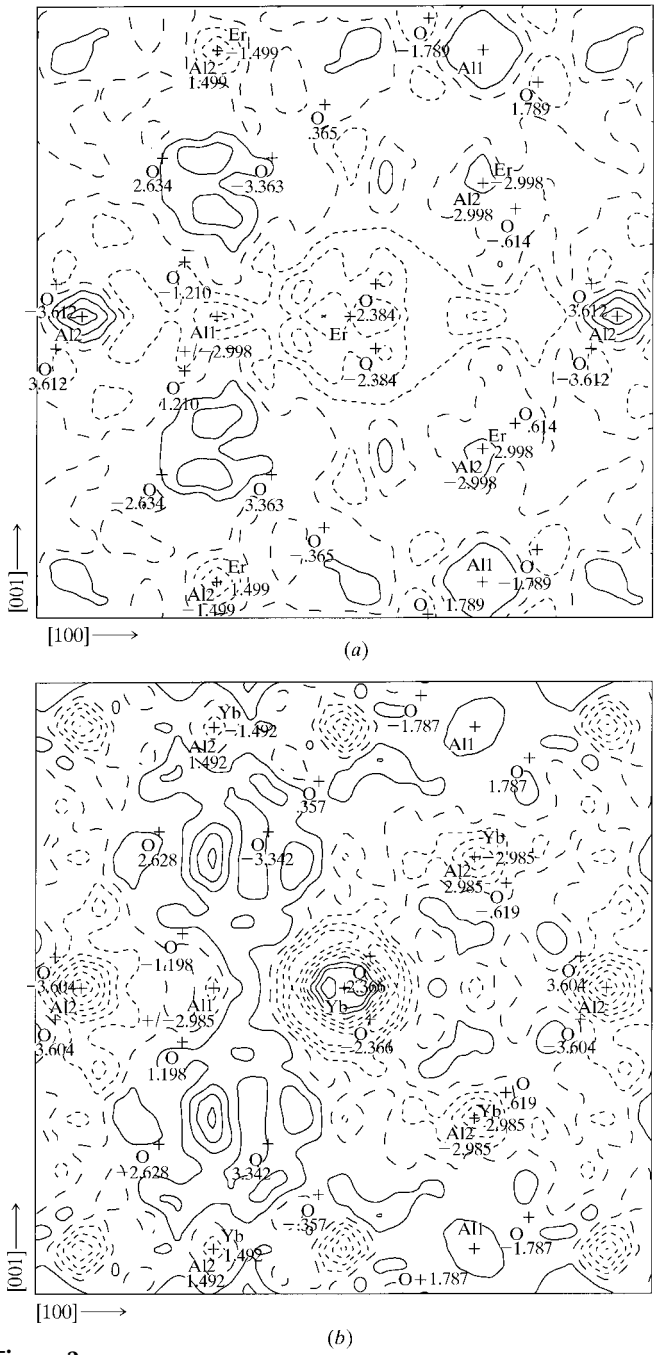

Figure 2
$\Delta\rho$ maps in the [010] plane for (*a*) $Er_3Al_5O_{12}$ and (*b*) $Yb_3Al_5O_{12}$. Contours as in Fig. 3. Map borders are 6.9 × 6.9 Å.

[1] Supplementary data for this paper are available from the IUCr electronic archives (Reference: OS0064). Services for accessing these data are described at the back of the journal.

Table 2
Selected interatomic distances (Å) and angles (°) in $Er_3Al_5O_{12}$ and $Yb_3Al_5O_{12}$.

		$Er_3Al_5O_{12}$	$Yb_3Al_5O_{12}$
RE—O	4	2.3051 (7)	2.2887 (9)
RE—O^{i}	4	2.4287 (8)	2.4105 (10)
RE—Al(2)	2	2.9982 (5)	2.9846 (2)
RE—Al(1)	6	3.35209 (5)	3.3369 (1)
RE—RE^{ii}	4	3.6720 (1)	3.65538 (16)
Al(1)—O	6	1.9261 (7)	1.9244 (9)
Al(2)—O^{iv}	4	1.7686 (7)	1.7627 (9)
O—RE—O		67.76 (3)	67.98 (3)
		72.11 (3)	72.19 (3)
		73.78 (3)	73.35 (3)
		94.96 (3)	95.12 (3)
		111.95 (3)	111.70 (3)
		124.85 (2)	124.91 (3)
		158.97 (3)	159.39 (3)
O—RE—Al(2)		36.05 (2)	36.10 (2)
		143.95 (2)	143.90 (2)
O—Al(1)—O		86.55 (3)	86.17 (4)
		93.45 (3)	93.83 (4)
O—Al(2)—O^{iv}		100.18 (3)	99.81 (4)
		114.30 (4)	114.51 (5)
O—Al(2)—RE		50.09 (2)	49.91 (3)
		129.91 (2)	130.09 (3)
Al(2)—O—Al(1)		130.21 (4)	129.61 (6)
Al(2)—O—RE		93.85 (3)	94.00 (4)
Al(2)—O—RE^{v}		121.25 (4)	121.54 (5)
Al(1)—O—RE		104.43 (3)	104.42 (4)
Al(1)—O—RE		100.02 (3)	100.07 (4)
RE—O—RE		101.71 (3)	102.10 (4)

Symmetry codes: (i) $z, -x, \frac{1}{2}-y$; (ii) $y, -z, \frac{1}{2}-x$; (iii) $\frac{1}{4}+y, \frac{1}{4}+x, \frac{1}{4}+z$; (iv) $\frac{1}{4}-x, \frac{1}{4}-z, \frac{1}{4}-y$; (v) y, z, x.

4. Electron density

The difference density maps for $Er_3Al_5O_{12}$ and $Yb_3Al_5O_{12}$ (Figs. 2 and 3) are those obtained after an isotropic Zachariasen extinction correction was applied. It should be noted that virtually identical $\Delta\rho$ maps resulted when an isotropic BCI extinction correction was applied. After applying an isotropic BCII correction, the positive contours around the rare earths were eliminated, the negative contours increasing by a factor of approximately two. The negative contours around Al(2) increased by a factor of approximately 1.5 (Er garnet) and 2.5 (Yb garnet), while the negative contours around Al(1) were halved. The large central depletion between the three rare-earth atoms in Fig. 3 was increased by a factor of 0.25 and 0.33 for the Er and Yb garnets, respectively.

The difference density maps for $Er_3Al_5O_{12}$ and $Yb_3Al_5O_{12}$ are similar, having accumulations and depletions of electron density at roughly the same locations. This was expected as the 4*f* electrons are shielded and cannot participate strongly in chemical bonding (*e.g.* Chatterjee *et al.*, 1988). Furthermore, Er and Yb are in close vicinity in the periodic table, with atomic numbers 68 and 70, respectively.

Views of the $\Delta\rho$ in the RE_3 planes, in the section parallel to the $(\bar{1}11)$ plane, for $Er_3Al_5O_{12}$ and $Yb_3Al_5O_{12}$ are depicted in Figs. 3(*a*) and (*b*), respectively. The large central electron depletion can be attributed to the quantum mechanical exchange effects between the three rare-earth atoms, the excess electrons being pushed aside into previously electron-deficient regions. The large electron density accumulation beside the RE–RE vector is nearly equidistant between the RE and Al(1) (∼2.17 and 2.23 Å, respectively, for $Er_3Al_5O_{12}$ and ∼2.14 and 2.17 Å, respectively, for $Yb_3Al_5O_{12}$).

Figs. 2(*a*) and (*b*) depict the difference electron density on the (010) plane for $Er_3Al_5O_{12}$ and $Yb_3Al_5O_{12}$. The electron density is depleted along the Al(2)—RE—Al(2) vector, with a

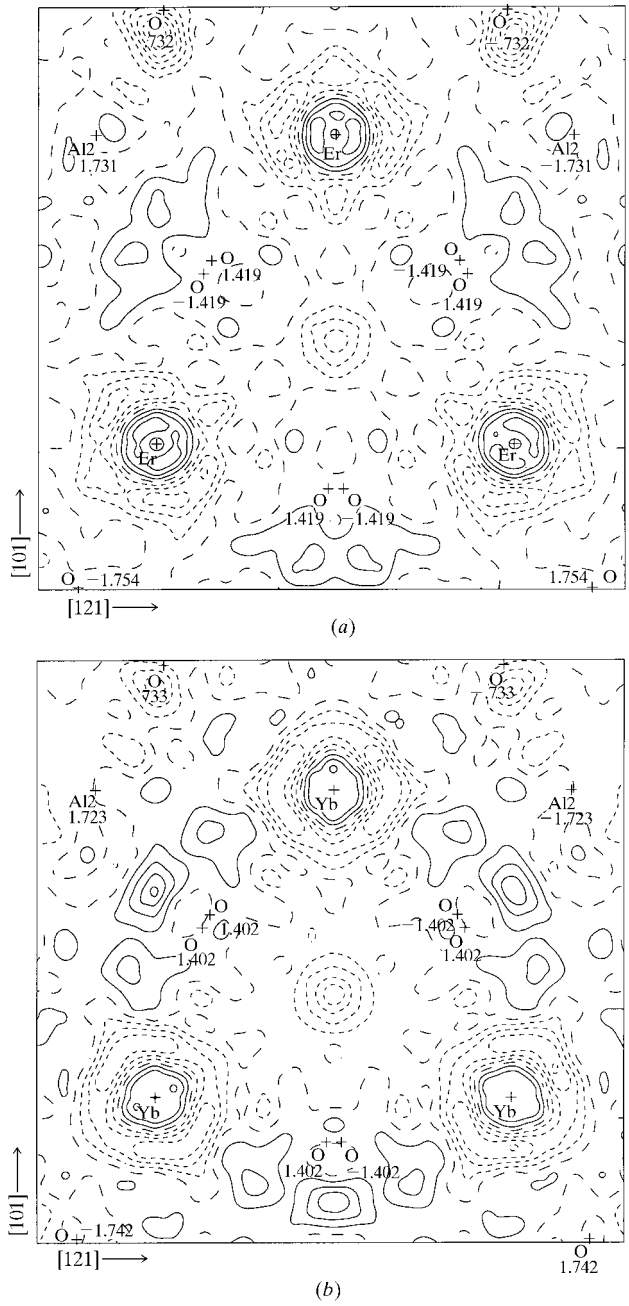

Figure 3
$\Delta\rho$ maps in the [111] plane for (*a*) $Er_3Al_5O_{12}$ and (*b*) $Yb_3Al_5O_{12}$. Contour intervals are 0.5 e Å^{-3}; positive contours are solid and negative contours are shown as short dashed lines. Map borders are 6.0 × 6.0 Å. The values near the atom labels indicate the distance from the plane.

slight accumulation of electrons in the region between the O atoms projected onto the plane. These are regions of depleted density along the Al(2)—RE—Al(2) vector, which are not associated with atomic positions.

The crystallographic point symmetry of the rare-earth site is 2.22 and reflects the oxygen coordination of the rare earth. However, the symmetry of the local $\Delta\rho$ around the rare earth is approximately *mmm*, which is higher than the crystallographic symmetry (*e.g.* Figs. 2*a* and *b*). This higher symmetry is induced by the next nearest cations rather than the oxygen array projected on the map's plane. It is interesting to note that the areas of depleted electron density between the rare-earth and the Al(2) atoms correspond to the electron accumulations on the Al(1) atom and between the O atoms projected on the map. The metal–O first coordination sphere, which reflects the crystallographic symmetry, is competing with the second nearest-neighbor metal–metal interactions. These metal–metal interactions have been noticed previously in studies by Maslen *et al.* (1993) for α-Al_2O_3, Hsu (1995) for $LiTaO_3$, du Boulay (1996) for $GaAlO_3$, Maslen *et al.* (1996) for RE_2O_3 and Lobanov *et al.* (1989). This effect would be considerably more pronounced if Fe was present rather than Al, as observed in $REAlO_3$ and $REFeO_3$ perovskites (*e.g.* du Boulay, 1996; du Boulay *et al.*, 1995; Maslen *et al.*, 1996).

This work was supported by the Australian Research Council. Financial support from the Australian Synchrotron Research Program funded by the Commonwealth of Australia *via* the Major National Research Facilities Program is also acknowledged.

References

Alcock, N. W. (1974). *Acta Cryst.* A**30**, 332–335.
Boulay, D. du (1996). PhD dissertation. Department of Physics, The University of Western Australia.
Boulay, D. du, Maslen, E. N., Streltsov, V. A. & Ishizawa, N. (1995). *Acta Cryst.* B**51**, 921–929.
Chatterjee, A., Maslen, E. N. & Watson, K. J. (1988). *Acta Cryst.* B**44**, 386–395.
Creagh, D. C. (1995/1996). Private communication.
Dana, E. S. (1954). *A Textbook of Mineralogy*, revised and enlarged by W. E. Ford, 4th ed. New York: John Wiley & Sons.
Garton, G. & Wanklyn, B. M. (1967). *J. Cryst. Growth*, **1**, 164–166.
Geller, S. (1967). *Z. Kristallogr.* **125**, 1–47.
Hall, S. R., King, G. S. D. & Stewart, J. M. (1995). Editors. *Xtal3.4 User's Manual.* University of Western Australia, Lamb, Perth, Australia, and Maryland, USA.
Hester, J. R., Maslen, E. N., Spadaccini, N., Ishizawa, N. & Satow, Y. (1993*a*). *Acta Cryst.* B**49**, 842–846.
Hester, J. R., Maslen, E. N., Spadaccini, N., Ishizawa, N. & Satow, Y. (1993*b*). *Acta Cryst.* B**49**, 967–973.
Hirshfeld, F. L. (1977). *Isr. J. Chem.* **16**, 198–201.
Hsu, R. M. (1995). Ph.D. Dissertation. Department of Physics, The University of Western Australia.
Hyde, B. G. & Andersson, S. (1989). *Inorganic Crystal Structures.* John Wiley and Sons, USA.
Kishimoto, S. (1995). *Rev. Sci. Instrum.* **66**, 2314–2316.
Lobanov, N. N., Butman, L. A. & Tsirel'son, V. G. (1989). *J. Struct. Chem.* **30**, 96–104 (English edition), 113–121 (Russian edition).
Maslen, E. N., Streltsov, V. A. & Ishizawa, N. (1996). *Acta Cryst.* B**52**, 414–422.
Maslen, E. N., Streltsov, V. A., Streltsova, N. R. & Ishizawa, N. (1995). *Acta Cryst.* B**51**, 929–939.
Maslen, E. N., Streltsov, V. A., Streltsova, N. R., Ishizawa, N. & Satow, Y. (1993). *Acta Cryst.* B**49**, 973–980.
O'Keeffe, M. & Hyde, B. G. (1981). *Structure and Bonding in Crystals*, Vol. I. New York: Academic Press.
Ramos-Gallardo, A. & Vegas, A. (1997). *J. Solid State Chem.* **128**, 69–72.
Rees, B. (1977). *Isr. J. Chem.* **16**, 180–186.
Remeika, J. P. & Kometani, T. Y. (1968). *Mater. Res. Bull.* **3**, 895–900.
Rubenstein, C. B. & Barns, R. L. (1964). *Am. Mineral.* **49**, 1489–1490.
Rubenstein, C. B. & Barns, R. L. (1965). *Am. Mineral.* **50**, 782–785.
Satow, Y. & Iitaka, Y. (1989). *Rev. Sci. Instrum.* **60**, 2390–2393.
Streltsov, V. A., Ishizawa, N. & Kishimoto, S. (1998). *J. Synchrotron Rad.* **5**, 1309–1316.
Wyckoff, R. W. G. (1963). *Crystal Structures*, Vol. 1, 2nd ed. New York: Interscience Publishers.
Zachariasen, W. H. (1967). *Acta Cryst.* **23**, 558–564.